UC Santa Barbara
UC Santa Barbara Previously Published Works

Title

Distal amyloid β-protein fragments template amyloid assembly

Permalink

https://escholarship.org/uc/item/3590w44j

Journal

Protein Science, 27(7)

ISSN

0961-8368

Authors

D., Thanh
Sangwan, Smriti
de Almeida, Natália EC
et al.

Publication Date

2018-07-01

DOI

10.1002/pro.3375

Peer reviewed

Distal amyloid β-protein fragments template amyloid assembly

Thanh D. Do [ID],[1] Smriti Sangwan,[2] Natália E. C. de Almeida,[1]
Alexandre I. Ilitchev,[1] Maxwell Giammona,[1] Michael R. Sawaya,[2]
Steven K. Buratto,[1] David S. Eisenberg,[2] and Michael T. Bowers[1]*

[1]Department of Chemistry and Biochemistry, University of California, Santa Barbara, California
[2]Departments of Chemistry and Biochemistry and Biological Chemistry, Howard Hughes Medical Institute, UCLA-DOE Institute for Genomics and Proteomics, University of California, 611 Charles Young Drive East, Los Angeles, California

Abstract: Amyloid formation is associated with devastating diseases such as Alzheimer's, Parkinson's and Type-2 diabetes. The large amyloid deposits found in patients suffering from these diseases have remained difficult to probe by structural means. Recent NMR models also predict heterotypic interactions from distinct peptide fragments but limited evidence of heterotypic packed sheets is observed in solution. Here we characterize two segments of the protein amyloid β (Aβ) known to form fibrils in Alzheimer's disease patients. We designed two variants of Aβ(19–24) and Aβ(27–32), IFAEDV (I6V) and NKGAIF (N6F) to lower the aggregation propensity of individual peptides while maintaining the similar interactions between the two segments in their native forms. We found that the variants do not form significant amyloid fibrils individually but a 1:1 mixture forms abundant fibrils. Using ion mobility-mass spectrometry (IM-MS), hetero-oligomers up to decamers were found in the mixture while the individual peptides formed primarily dimers and some tetramers consistent with a strong heterotypic interaction between the two segments. We showed by X-ray crystallography that I6V formed a Class 7 zipper with a weakly packed pair of β-sheets and no segregated dry interface, while N6F formed a more stable Class 1 zipper. In a mixture of equimolar N6F:I6V, I6V forms a more stable zipper than in I6V alone while no N6F or hetero-typic zippers are observed. These data are consistent with a mechanism where N6F catalyzes assembly of I6V into a stable zipper and perhaps into stable, pure I6V fibrils that are observed in AFM measurements.

Keywords: amyloid; aggregation; co-assembly; ion-mobility mass spectrometry; X-ray crystallography

Introduction

The formation of amyloidogenic, proteinaceous fibrils has applications in both materials[1–3] and biological science.[4–7] However, it is this latter application that interests us here, due to amyloids being associated with devastating diseases such as Alzheimer's, Parkinson's and Type-2 Diabetes.[4–7] Biological amyloidogenic structures are characterized by the assembly of hundreds to thousands of monomer subunits into a thermodynamically stable fiber-like structure.[4–6] The classical amyloid β (Aβ) fibrils found in the brains of Alzheimer's disease patients have a relatively

uniform 10 nm diameter and the presence of amyloid fibrils is strongly correlated with the disease.[7] Full-length Aβ is natively disordered and aggregation prone, encompassing multiple segments capable of nucleating fibril growth.[8,9] Prior research has isolated different fibril assemblies termed polymorphs that differ in morphology, structure and seeding capacities.[8–11] These polymorphs are increasingly found to have prion-like characteristics as one polymorph can propagate indefinitely in vitro[11–13] and in vivo.[9,14–17] Crystal structures of shorter segments have thus far only yielded homotypic steric zippers - two self-complementary β-sheets, giving rise to the spine of an amyloid fibril - although there is evidence from NMR studies[9,18–25] and cyroEM[26] that different segments can indeed form heterotypic interactions. (Here we note that the term "heterotypic" used in this work describes interactions between distinct peptides/protein fragments with no intramolecular linkage). It has also been proposed that distal Aβ segments can associate to form the spines of amyloid fibrils, yielding an aggregate morphology different from those of individual segments.[9] However, there has not yet been detailed supporting evidence from structural analysis. Such an aggregation cascade might involve structural rearrangement at an early oligomer level or more likely the formation of oligomers capable of nucleating self-assembly of unstructured monomers.[27] An understanding of this assembly process and possible hetero-fibrillar structures can provide insight for development of potential therapeutic strategies for neurodegenerative diseases[28] as well as new scaffolds for biomaterials.[1–3] Here our priority is to investigate the interactions between distinct Aβ peptide fragments in solution that do not themselves form fibrils and determine whether fibril formation can be observed in the mixture. Recently several high resolution NMR structures of full-length Aβ(1–40) and Aβ(1–42) were reported by the Glockshuber, Meier, Riek, Tycko, and Griffin laboratories.[21–25,29,30] These NMR structures showed detailed interactions between different β-sheet segments created by the stacking of monomers in a specific conformation. They also included the identities of residues forming salt-bridges and hydrophobic interactions revealing subtle differences in the assembly of Aβ(1–40), Aβ(1–42) and their familial mutants. Hence, the heterotypic interactions between β-sheets are unambiguously critical for the aggregation and self-assembly of the full-length Aβ.

Previous studies have shown that when a peptide with a strong aggregation propensity is mixed with a weakly aggregating peptide, the heterotypic interactions lead to aggregation inhibition despite the formation of hetero-oligomers.[31,32] Hence, in order to promote possible heterotypic assembly the pair of peptides must both be weakly aggregating and the heterotypic pair potentially strongly aggregating. Possible driving forces for peptide association can arise from hydrophobic[33,34] or electrostatic interactions,[35,36] hydrogen bonding and π-stacking,[37] each of which must be considered in selecting a system capable of heterotypic assembly.

A recent NMR study by Nowick and co-workers of cyclic peptides derived from Aβ(17–23) and Aβ(30–36) by unnatural amino acid modification showed that co-assembly can occur[38] but evidence of such an interaction in native peptides (without cyclization and unnatural amino acid modification) in solution is lacking. Here, we use a combination of ion-mobility mass spectrometry (IM-MS), X-ray crystallography and atomic force microscopy (AFM) to investigate the co-aggregation of two mutated Aβ segments residing on the opposite sides of the loop in the strand-loop-strand monomeric state of an aggregating Aβ(1–42)[30,39] that is found in the loop region of Aβ(1–42) fibrils.

Results and Discussion

Aβ hexapeptide selection and mutation

The first step of our study is to come up with possible peptide fragments having poor aggregation propensities but may assist fibril growth when incubated together. We utilized ZipperDB (https://services.mbi.ucla.edu/zipperdb/),[40,41] that had been successfully used in the past,[42,43] to search for two Aβ hexapeptides that satisfy three conditions: (a) contain pairs of hydrophobic residues (e.g., isoleucine, leucine, phenylalanine, etc.) that can nucleate aggregation,[36,44] (b) possess opposite net charges to reduce aggregation propensities of individual peptides and to make association favourable,[33,34] and (c) have Rosetta Energy (RE) of approximately −20 kcal/mol (the NNQQNY peptide model has an RE of −23 kcal/mol, and aggregates relatively weakly in water[43]). Briefly, each six-residue segment (not containing a proline) from the protein sequence is threaded onto the NNQQNY structure backbone, and the energetic fit is evaluated by using the RosettaDesign program.[45] Additionally, the segments should possess some native interactions in the context of full-length Aβ. There are two Aβ hexapeptides (see Fig. S1) that meet these requirements: Aβ(19–24) ([19]FFAEDV,[24] RE = −19.3 kcal/mol) and Aβ(27–32) ([27]NKGAII,[32] RE = −23.5 kcal/mol), both located in the loop region of Aβ in its fibrillar form according to the atomic models obtained from previous X-ray[39] and NMR studies (Fig. 1).[18,20,46]

Previous NMR studies by Tycko, Smith, and co-workers suggested that the salt-bridge between Asp 23 and Lys 28 is critical for Aβ(1–40) (the most dominant isoform of Aβ)[47,48] to adopt a strand-loop-strand structure.[49] Also in Aβ(1–40), a similar structure is stabilized by hydrophobic interactions between Phe 19 and Ile 32[30,49,50] and hence we chose the second fragment [27]NKGAII[32] to contain

Aβ(1-42): DAEFR⁵HDSGY¹⁰EVHHQ¹⁵KLVFF²⁰AEDVG²⁵SNKGA³⁰IIGLM³⁵VGGVV⁴⁰IA

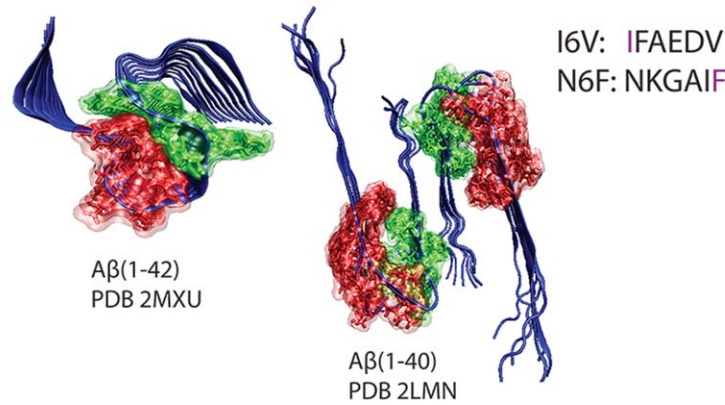I6V: IFAEDV
N6F: NKGAIF

Aβ(1-42)
PDB 2MXU

Aβ(1-40)
PDB 2LMN

Figure 1. Aβ(1–42) primary sequence and fibril structures of Aβ(1–42) and Aβ(1–40) obtained from solid-state NMR (PDB 2MXU and PDB 2LMN, respectively). Aβ(19–24) and Aβ(27–32) segments are shown in red and green, respectively.

Lys28 and Ile32. This peptide was previously shown to form fibrils.[9] Therefore, we decided to make a single mutation on each peptide fragment to weaken the aggregation propensity of Aβ(27–32) while maintaining the overall identity of the amino acids. The mutation made on each peptide, I6V (IFAEDV, RE = −17.8 kcal/mol) and N6F (NKGAIF, RE = −23.7 kcal/mol), allowed π-stacking to be weakened in homo-oligomers but be strengthened in hetero-association. Of note, N6F has lower Rosetta energy than I6V, suggesting higher aggregation propensity but as we will show it only forms a small amount of short fibrillar aggregates.[40,41]

N6F and I6V have poor aggregation propensities individually but an equimolar mixture forms abundant fibrils

We evaluated the aggregation propensity of incubated I6V and N6F samples using atomic force microscopy (AFM). Figure 2(A,B) shows representative AFM images obtained from the pure I6V and N6F samples after 2-day incubation in water at 250 μM. I6V peptide [Fig. 2(A) and Fig. S2] formed only spherical aggregates with an average height of 2.25 nm and no mature fibrils. N6F peptide [Fig. 2(B) and Fig. S3] also formed spherical aggregates (average height = 2.5 nm) in addition to some short and branched fibrils. These observations are consistent with the Rosetta energy scores suggesting that the fibril formation propensy of N6F is higher than that of I6V. Next, we aggregated the peptides together in a 1:1 stoichiometric ratio. Long fibrils (4.0–6.0 nm in height) are abundantly visible in the AFM image of the mixture [Fig. 2(C): Note the length axis is 10 times that of Fig. 2(A) and 2(B)]. These data indicate that interactions between I6V and N6F can promote fibril formation that is otherwise limited in the pure samples.

We used a Thioflavin-T (ThT) assay to qualitatively compare the β-sheet content in the pure samples of I6V and N6F to their mixture (see Fig. S4). The increase in ThT fluorescence intensity upon fibril binding makes it a sensitive and efficient reporter. The β-sheet content of I6V is much lower
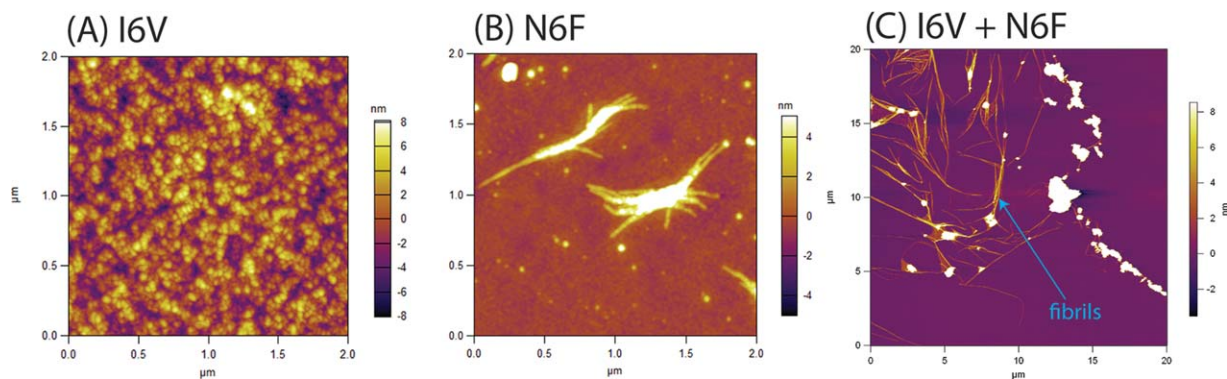

Figure 2. Representative AFM images of I6V and N6F incubated for 2 days at 250 μM in water. (A) I6V shows the formation of spherical aggregates, (B) N6F forms a mixture of spherical and short fibrillar aggregates, and (C) the mixture of I6V and N6F populates long fibrils. The scale of panel C is an order of magnitude larger than the other two panels (20 × 20 μm² vs. 2 × 2 μm²) to illustrate that the aggregation in the mixture had led to the formation of long amyloid-like fibrils and the phenomenon is not region-specific.
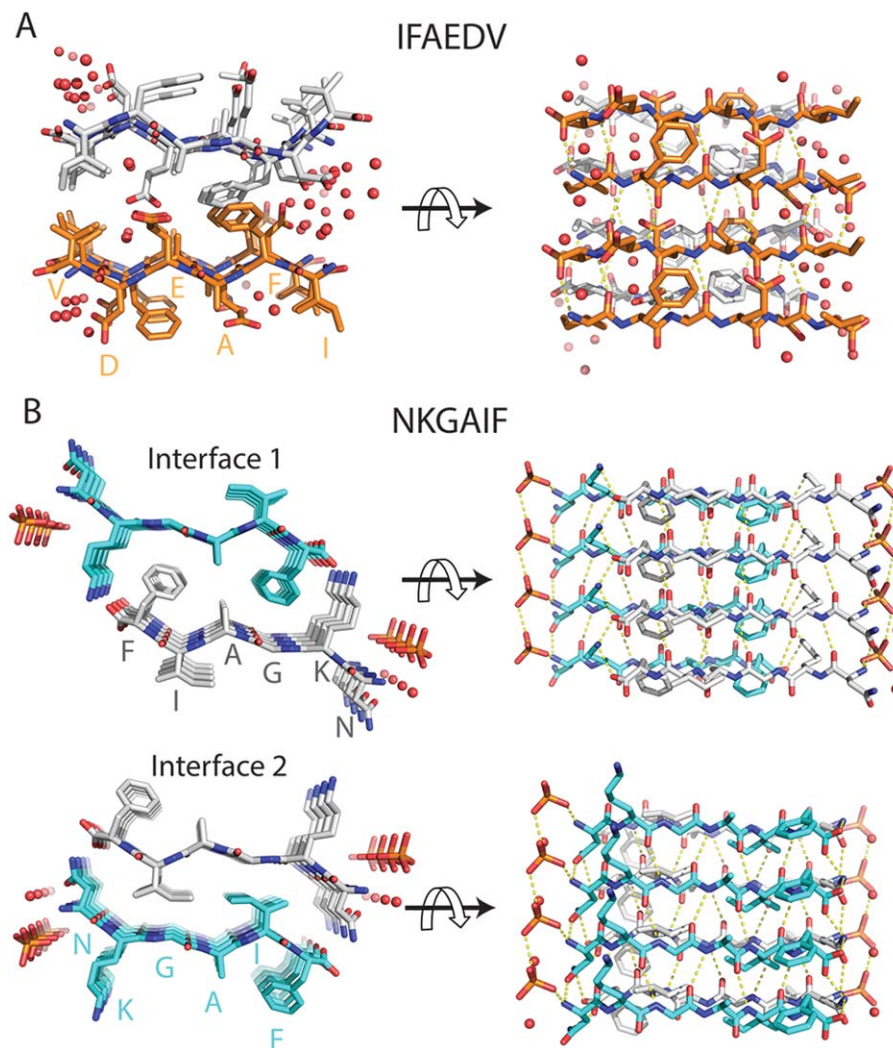
Figure 3. (A) I6V (IFAEDV) forms a Class 7 zipper. Water molecules are colored in red and each sheet in gray and orange. Hydrogen bonding along the sheet is shown on the right. (B) N6F (NKGAIF) forms a Class 1 zipper. The crystal structure shows two different interfaces encapsulating a dry interior. Phosphate and water molecule are colored orange and red.

than N6F, which is consistent with their RE (−17.8 kcal/mol vs. −23.7 kcal/mol). In the mixture, the β-sheet content increases to the same level as that of the pure N6F. We note that ThT is only sensitive to β-sheet formation, which is a necessary but not a sufficient condition for fibril formation. We will further explain this observation in light of IM-MS and X-ray crystallography data presented below.

Crystal structures of I6V and N6F reveal different steric zippers

To gain atomic resolution insight into the packing polymorphism of these peptides, we used X-ray crystallography. The peptides were put in crystallization trials individually and in a 1:1 mixture (X-ray diffraction and refinement statistics can be found in Table S1). Both peptides formed needle-like microcrystals and their structures were determined. I6V crystal structure [Fig. 3(A)] shows anti-parallel β-

strands stacked face-to-back. Two sheets interact with each other via interactions between Glu 4 and Phe 2. It is a Class 7 zipper[8] with water molecules present between the mating sheets as well as outside. Since Glu 4 is a charged residue and Phe 2 is a hydrophobic aromatic residue, the interaction between the two sheets is relatively weak. The sheets also do not display segregated dry and wet interfaces as seen in typical amyloid steric zippers.[8,44]

Since the early report by Sawaya et al.,[8] several steric zipper crystal structures were solved by the Eisenberg laboratory including not only strongly aggregating peptides, but also some weakly aggregating peptides.[44] We have shown that while the formation of a steric zipper is critical for fibril formation, the propensity strongly depends on the stability of the zipper structures.[44] From Figure 3(A), the presence of weakly packed sheets in I6V suggests that resulting fibrils would not be strongly

bound and the formation of globular aggregates could well be competitive in solution.[51]

The N6F crystal structure [Fig. 3(B)] shows parallel β-strands stacked via main carbon chain hydrogen bonding forming a tight hydrophobic interface; a Class 1 zipper.[8] There are two different interfaces encapsulating dry interiors. The mating β-sheets are tightly packed via face-to-face interactions between Phe 6 and Ala 4 or back-to-back interactions between Ile 5 from mating sheets. Both interfaces have high shape complementarity (Sc; 0.88 and 0.85) and large buried surface area (Ab; 324 and 312 Å^2). The atomic structure of N6F is identical to the atomic structure of the native ^{27}NKGAII^{32} structure that was previously determined[9] with the two interfaces intact. Since previous work showed that NKGAII formed fibrils,[9] and here we showed that N6F adopts identical steric zipper structures but formed only a few short fibrils, the mutation indeed decreased the aggregation propensity of this peptide as we expected. Furthermore, our ThT-assay showed that the mixture has similar β-sheet content as N6F, indicating that the oligomers (which could be either homo or hetero-oligomers) in the mixture have similar β-sheet content to N6F, but probably adopt a different steric zipper polymorph as they can later form fibrils.

Comparing the two crystal structures, N6F has almost twice the Ab of I6V (324 Å^2 vs. 172 Å^2) and also higher Sc (0.88 vs. 0.66) suggesting a stable interaction and higher aggregation propensity[44] in agreement with our AFM data where some short fibrils are observed competing with globular aggregates.

IM-MS data reveal stable, β-rich hetero-oligomer formation by the two peptides

Next, we turned to IM-MS to characterize the early oligomer formation of the segments in isolation and in the mixture. Since the natural charge state of I6V is −2 and that of N6F is +1, we performed IM-MS experiments in both positive and negative polarity. Figure 4(A–C) shows the mass spectra of I6V, N6F and the mixture obtained in negative mode MS. Each peak is annotated with the oligomer number to charge ratio. The data obtained in positive mode are shown in Figures S5 and S6 and additional data in negative mode are shown in Figures S7 and S8. The oligomer composition of each of the mass spectral peaks can be determined by obtaining their arrival time distributions (ATDs) with an example given in Figure 4(F). From these experiments we determine that negative mode IM-MS of pure I6V and N6F samples show the formation of monomers, dimers and tetramers, whereas positive mode IM-MS shows at most dimer.

Further analyses of the dimer and tetramer cross sections reveal that both peptides form

globular, non β-sheet oligomers in the IM-MS data and their cross sections are in good agreement with the isotropic model[51] [$\sigma_n = \sigma_1 \times n^{2/3}$, see Fig. 4(D,E) and also Table S2 and S3]. This data is consistent with our microscopy data showing I6V formed only globular aggregates.[43,51] There is a small deviation at the tetramer stage of N6F, consistent with the fact this peptide formed some short fibrils [Fig. 2(B)]. The presence of limited, non β-sheet oligomers is consistent with a low propensity to aggregate for both peptides.

When the two peptides are mixed, large hetero-oligomers up to decamers are detected in both negative [Fig. 4(C)] and positive polarity (Fig. S6). In negative mode, there are mass spectral peaks corresponding to hetero-dimer $(p + q)/z = (1 + 1)/{-1}$ at m/z 1342, hetero-tetramer $(3 + 1)/{-2}$ at m/z 1364, and hetero-decamer $(5 + 5)/{-4}$ at m/z 1678, where p and q are the oligomer numbers of I6V and N6F, respectively and z is the total charge of the complex. More hetero-oligomers are found in the positive mode IM-MS data including dimer, trimer, pentamer, hexamer, and decamer. Starting at heterodimers, the calculated cross sections begin to deviate positively from the isotropic predictions, as shown in Figure 5.

Overall, we observed heteroligomers of the size of $n = 2$, 3, 4, 5, 6, and 10 in positive polarity and $n = 2$, 4, and 10 in negative mode polarity. For the heteroligomers with the same total oligomer number the compositions may be different as evidenced by different values of m/z, indicating that they are distinct species. Since I6V is negatively charged and N6F is positively charged in solution, performing IM-MS experiments in both polarities captured a range of different species. Heteroligomers at other sizes may exist, but we couldn't capture them due to either abundance or the low mass resolution of the instrument used to obtain the negative polarity data.

The $(3 + 1)/{-2}$ tetramers [see Fig. 4(F)] adopt both a compact structure ($\sigma_{exp} = 447$ Å^2) and an extended, likely β-rich structure ($\sigma_{exp} = 550$ Å^2).[52] Furthermore, the mass spectral peaks corresponding to $(p + q)/z = (3 + 1)/{-2}$ and $p/z = 2/{-1}$ oligomers are more intense than their counterparts, namely $(p + q)/z = (1 + 3)/{-2}$ and $q/z = 2/{-1}$ [see Fig. 4(C)], which qualitatively suggests that I6V is more prone to form both homo- and hetero-oligomers than N6F in the equal molar mixture. This observation is important because it suggests that an incorporation of a small quantity of N6F assists the formation of non-isotropic I6V oligomers. In a recent study in which IM-MS was coupled to IR spectroscopy, we showed that oligomers that deviated positively from the isotropic prediction are β-rich structures.[52] Hence, N6F may be able to seed I6V structural assembly in the mixture that is not possible in the pure sample.
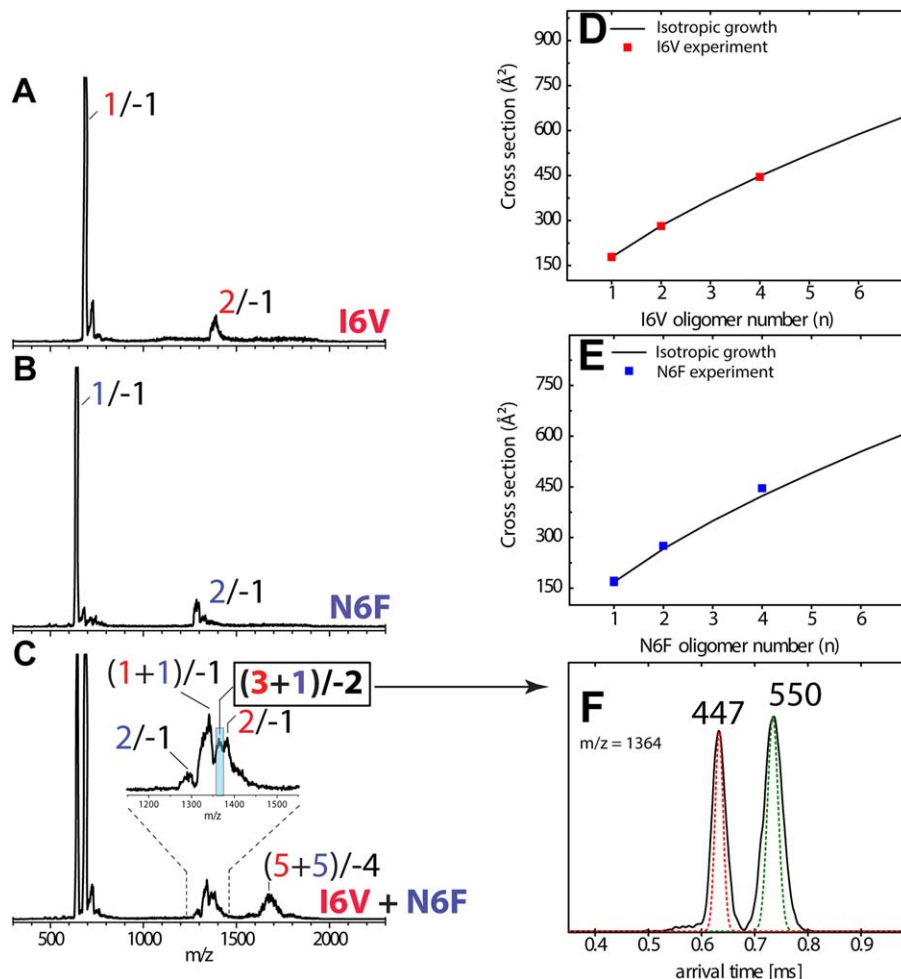
Figure 4. Negative ion nano-ESI-Q mass spectra of (A) I6V alone, (B) N6F alone, (C) I6V incubated with N6F at 1:1 molar ratio. The peptide concentrations were 150 μM (in 20 mM of ammonium acetate, pH 7.4). The peaks of I6V and N6F homo-oligomers are annotated with respect to their n/z where n is the oligomer number and z is the charge, whereas the I6V and N6F hetero complex peaks are reported as $(p + q)/z$ where p (in red) and q (in blue) are the oligomer numbers of I6V and N6F, respectively. The oligomer growth curves are given in (D) I6V homo-oligomers and (E) N6F homo-oligomers. (F) Representative ATD of hetero-tetramer composed of three I6V and one N6F. Cross section unit is $\mathring{A}^2$.

In general there are two plausible pathways for co-assembly of the two peptides. In the first pathway, the peptides co-assemble to form hetero-oligomers such that both I6V and N6F contribute relatively equally to fibril growth. The second pathway involves the formation of "seeded" fibrils resulting from one peptide (N6F) seeding the formation of I6V oligomers which subsequently form a new kind of steric zipper that nucleates fibrils of only I6V. More will be said on this shortly.

X-ray crystallography of the I6V and N6F mixture reveals a new polymorph of I6V

Crystallization trials of I6V and N6F mixed in equimolar amounts yielded crystals composed of I6V only, albeit in a different polymorph which we refer to as "form 2" (Fig. 6). No heterotypic structure of mixed I6V and N6F was obtained. I6V form 2 is a Class 8 steric zipper with a face to back orientation of mating sheets.[8] The interactions between Phe 2

and Glu 4 in form 1 are replaced by the same residue type interactions between opposite Phe 2 and Glu 4. While Phe–Phe interaction is favorable, Glu–Glu interaction places the two negative charges in close proximity. The shape complementarity and buried surface area (see Table I) of I6V "form 2" are higher than I6V "form 1" [Fig. 3(A)].

These X-ray crystallography data are consistent with a mechanism where N6F catalytically induces I6V to adopt a different class of steric zipper that is more stable than the zipper formed in neat I6V solutions. *Collectively all of the data provide both the observation of, and a possible mechanism for, the first example of linear peptide fragments derived from Aβ where facile fibril formation occurs in the mixture but very limited or no fibril formation occurs in the pure samples.*

To assess whether a fully heterotypic oligomer mechanism is plausible, rather than the catalytic mechanism mentioned above, two possible models of
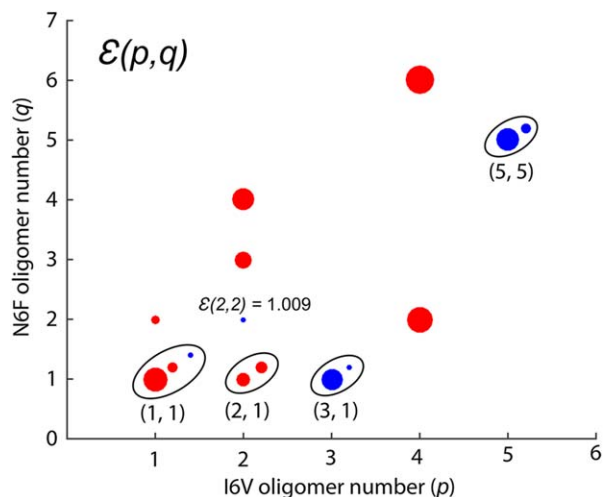
Figure 5. Scatter plot of the ratios of experiment to isotropic cross sections; $\varepsilon(p,q)$ for hetero-oligomers detected in positive (red) and negative (blue) mode IM-MS experiments. The size of each dot is scaled linearly with the values of $\varepsilon(p,q)$. The larger the dot size the greater the deviation from isotropic and hence the greater the β-sheet content.[43] The raw data can be found in Table S4 along with the method for determining dot size.

heterotypic I6V/N6F steric zipper were constructed and are given in Figure 7. In the first model (model A in Fig. 7), the steric zipper is formed by two mixed β-sheets in which I6V and N6F peptides intercalate each other. The zipper interface between the two mating sheets is similar to that of I6V form 1. One major difference is that in form 1 of I6V the side chains of Glu and Phe are in close proximity, which can create an anion-π interaction which is not favorable. In model A, such interactions are weakened since the two side chains are further away from each other. However, the Sc and Ab scores of this model are quite low; Sc = 0.69 and Ab = 172 Å^2, which are comparable to I6V form 1 (Sc = 0.66, Ab = 172 Å^2) but worse than I6V form 2 (Sc = 0.73, Ab = 208 Å^2).

In the second model (model B in Fig. 7), the steric zipper is composed of two homotypic sheets of I6V and N6F. In this case, the Glu residues of I6V peptides stack along the fibril axis. The presence of Glu in the zipper interface is thought to contribute negatively toward the stability of the zippers in both models. However, the Glu residues in our proposed models are either not interacting (model A) or stacked in one direction (model B). The Sc and Ab scores for this model are 0.65 and 204.9 Å^2, respectively, which are better than model A and I6V form 1, and comparable to I6V form 2. While this heterotypic zipper model might exist in solution we have no evidence for it as it was not captured in the crystallization trials, while the I6V form 2 zipper was captured supporting the N6F catalysis mechanism.

Summary and Conclusions

AFM, IM-MS, and X-ray crystallography were utilized to investigate fibril formation of neat hexapeptides designed from Aβ protein and a mixture containing the two hexapeptides. We have shown that Aβ hexapeptides that only weakly assemble on their own can interact heterotypically when mixed together and form fibrils and that β-sheet formation occurs early in the hetero-oligomer assembly process. Both negative and positive mode IM-MS detect large, non-isotropic heteroligomers composed of I6V and N6F peptides. In the pure peptides I6V is less aggregation prone than N6F. However, in the mixture I6V becomes more prone than N6F to form both homo- and hetero-oligomers. Structural studies with X-ray crystallography reveal a polymorphic form of I6V steric zipper (Class 8)[8] when crystals are formed from the mixture in support of the formation of more stable I6V homofibrils. The IM-MS data indicate that hetero-oligomers are readily formed in the mixture of I6V and N6F that are β-sheet rich. Hence, the data are consistent with a model in which N6F acts primarily as a catalyst in the
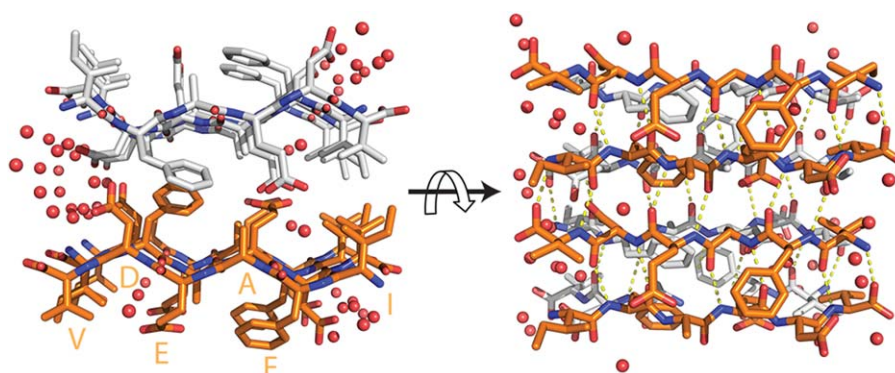

Figure 6. X-ray crystallography data of equal molar mixture of I6V and N6F. I6V forms a Class 8 zipper (form 2) in the presence of N6F. It composed of pair of anti-parallel β sheets. Water molecules are colored in red and each sheet in gray and orange.

Table I. *Shape Complementarity (Sc) and Buried Surface Area (Ab, Å^2) of the Different Structures Determined*[a]

Peptide and Model	IFAEDV (Form 1)	NKGAIF (Interface 1)	NKGAIF (Interface 2)	IFAEDV (Form 2)	Heterotypic Model A	Heterotypic Model B
Sc	0.658	0.877	0.845	0.725	0.470	0.69
Ab	172	324	312	208	172	205

[a] Notice that the form 2 of IFAEDV (crystallized in the presence of NKGAIF) has higher Sc and Ab compared to form 1. Ab was calculated using AREAIMOL by subtracting the solvent accessible area of one strand from a pair of sheets. Shape complementarity was calculated for a pair of sheets.

mixture of N6F and I6V promoting a new I6V steric zipper and perhaps pure I6V fibrils.

An interesting and important aspect of protein aggregation lies in the ability of different segments within a protein, or parts of different proteins to promote association and fibril formation. Our study provides an example of two distinct segments in Aβ protein that can promote fibril formation when mixed together. Our work has implications not only for the mechanism of folding and assembly in Aβ, but also in the design of intrinsically non-aggregating peptides that might carry a variety of functional probes and only assemble when mixed with another designed peptide. Such a strategy can have wide applications in materials research and in medical and environmental science.

Materials and Methods

A full description of methods is given in Supplementary Material. Briefly, for IM-MS samples were dissolved in water to the desired concentration, loaded into gold coated nanoESI capillaries, and electrosprayed on home-built instruments.[53,54] Positive mode data were collected on an IM-MS instrument consisting of a nano-electrospray source, an ion funnel, a 2-m long drift cell, an exit funnel and a quadrupole mass analyzer.[54] Negative mode data were collected on another IM-MS instrument having a shorter drift cell (∼5 cm).[53] In both cases, the ions are pulled through the drift tube under the influence of a weak electric field. At the end of the drift tube ions of a particular oligomeric state are mass selected and their arrival time distribution (ATD) is
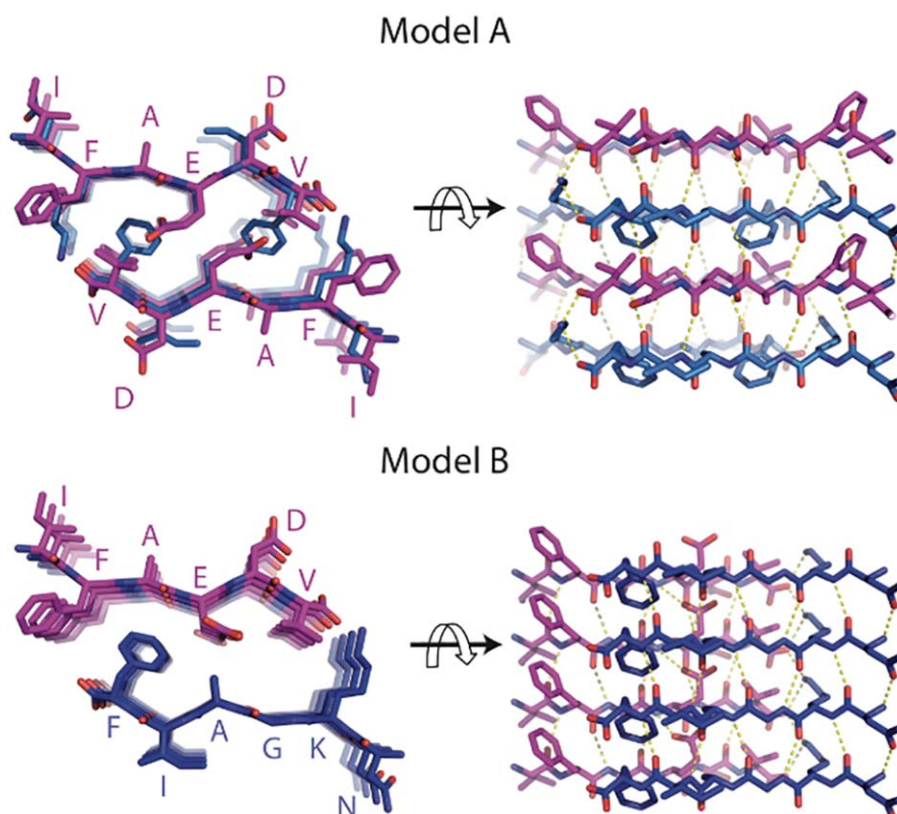

Figure 7. Proposed models of heterotypic N6F/I6V steric zippers. N6F is shown in blue and I6V is shown in magenta. In model A, the steric zipper is composed of two hetero-β mating sheets. In model B, the two mating sheets are homo β-sheets of I6V and N6F.

recorded. The arrival time is related to the collision cross-section of the ion (see Supplementary Material). For AFM images aliquots of the same peptide sample solutions were drop cast onto freshly cleaved mica slides and imaged on a MFP-3D-SA instrument (AsylumResearch, Santa Barbara). X-ray crystals of peptide solutions were grown in hanging drop VDX plates (Hampton Research, Aliso, Viejo, CA) and all data were collected at Advanced Photon Source (Chicago, IL) beam lines 24-ID-E. Atomic coordinates and structure factors have been deposited in the Protein Data Bank as 5TXD for N6F, 5TXJ for I6V, and 5TXH for I6V form 2.

Author Contributions

The manuscript was written through contributions of all authors.

Conflicts of Interest

The authors declare no conflict of interest.

Ackowledgments

References

1. Peralta MD, Karsai A, Ngo A, Sierra C, Fong KT, Hayre NR, Mirzaee N, Ravikumar KM, Kluber AJ, Chen X, Liu GY, Toney MD, Singh RR, Cox DL (2015) Engineering amyloid fibrils from beta-solenoid proteins for biomaterials applications. ACS Nano 9:449–463.

2. Knowles TPJ, Mezzenga R (2016) Amyloid fibrils as building blocks for natural and artificial functional materials. Adv Mater 28:6546–6561.

3. Knowles TPJ, Buehler MJ (2011) Nanomechanics of functional and pathological amyloid materials. Nat Nanotechnol 6:469–479.

4. Chiti F, Dobson CM (2006) Protein misfolding, functional amyloid, and human disease. Annu Rev Biochem 75:333–366.

5. Caughey B, Lansbury PT (2003) Protofibrils, pores, fibrils, and neurodegeneration: Separating the responsible protein aggregates from the innocent bystanders. Ann Rev Neurosci 26:267–298.

6. Eisenberg D, Jucker M (2012) The amyloid state of proteins in human diseases. Cell 148:1188–1203.

7. Westermark P, Andersson A, Westermark GT (2011) Islet amyloid polypeptide, islet amyloid, and diabetes mellitus. Physiol Rev 91:795–826.

8. Sawaya MR, Sambashivan S, Nelson R, Ivanova MI, Sievers SA, Apostol MI, Thompson MJ, Balbirnie M, Wiltzius JJW, McFarlane HT, Madsen AØ, Riekel C, Eisenberg D (2007) Atomic structures of amyloid cross-b spines reveal varied steric zippers. Nature 447:453–457.

9. Colletier J-P, Laganowsky A, Landau M, Zhao M, Soriaga AB, Goldschmidt L, Flot D, Cascio D, Sawaya MR, Eisenberg D (2011) Molecular basis for amyloid-β polymorphism. Proc Natl Acad Sci USA 108:16938–16943.

10. Nelson R, Sawaya MR, Balbirnie M, Madsen AO, Riekel C, Grothe R, Eisenberg D (2005) Structure of the cross-beta spine of amyloid-like fibrils. Nature 435:773–778.

11. Lu JX, Qiang W, Yau WM, Schwieters CD, Meredith SC, Tycko R (2013) Molecular structure of beta-amyloid fibrils in Alzheimer's disease brain tissue. Cell 154:1257–1268.

12. Petkova AT, Leapman RD, Guo Z, Yau WM, Mattson MP, Tycko R (2005) Self-propagating, molecular-level polymorphism in Alzheimer's beta-amyloid fibrils. Science 307:262–265.

13. Goldsbury C, Frey P, Olivieri V, Shirley UA, Müller A (2005) Multiple assembly pathways underlie amyloid-b fibril polymorphisms. J Mol Biol 352:282–298.

14. Wiltzius JJW, Landau M, Nelson R, Sawaya MR, Apostol MI, Goldschmidt L, Soriaga AB, Cascio D, Rajashankar K, Eisenberg D (2009) Molecular mechanisms for protein-encoded inheritance. Nat Struct Mol Biol 16:973–998.

15. Stohr J, Watts JC, Mensinger ZL, Oehler A, Grillo SK, DeArmond SJ, Prusiner SB, Giles K (2012) Purified and synthetic Alzheimer's amyloid beta (Abeta) prions. Proc Natl Acad Sci USA 109:11025–11030.

16. Walker LC, Schelle J, Jucker M (2016) The prion-like properties of amyloid-beta assemblies: Implications for Alzheimer's disease. Cold Spring Harb Perspect Med 6:a024398.

17. Ye L, Fritschi SK, Schelle J, Obermuller U, Degenhardt K, Kaeser SA, Eisele YS, Walker LC, Baumann F, Staufenbiel M, Jucker M (2015) Persistence of Abeta seeds in APP null mouse brain. Nat Neurosci 18:1559–1561.

18. Lührs T, Ritter C, Adrian M, Riek-Loher D, Bohrmann B, Döbeli H, Schubert D, Riek R (2005) 3D structure of Alzheimer's amyloid-beta(1–42) fibrils. Proc Natl Acad Sci USA 102:17342–17347.

19. Nelson R, Eisenberg D (2006) Recent atomic models of amyloid fibril structure. Curr Opin Struct Biol 16:260–265.

20. Petkova AT, Ishii Y, Balbach JJ, Antzutkin ON, Leapman RD, Delaglio F, Tycko R (2002) A structural model for Alzheimer's beta-amyloid fibrils based on experimental constraints from solid state NMR. Proc Natl Acad Sci USA 99:16742–16747.

21. Walti MA, Ravotti F, Arai H, Glabe CG, Wall JS, Bockmann A, Guntert P, Meier BH, Riek R (2016) Atomic-resolution structure of a disease-relevant Abeta(1–42) amyloid fibril. Proc Natl Acad Sci USA 113:E4976–E4984.

22. Colvin MT, Silvers R, Ni QZ, Can TV, Sergeyev I, Rosay M, Donovan KJ, Michael B, Wall J, Linse S, Griffin RG (2016) Atomic resolution structure of

monomorphic Abeta42 amyloid fibrils. J Am Chem Soc 138:9663–9674.

23. Tuttle MD, Comellas G, Nieuwkoop AJ, Covell DJ, Berthold DA, Kloepper KD, Courtney JM, Kim JK, Barclay AM, Kendall A, Wan W, Stubbs G, Schwieters CD, Lee VM, George JM, Rienstra CM (2016) Solid-state NMR structure of a pathogenic fibril of full-length human alpha-synuclein. Nat Struct Mol Biol 23:409–415.

24. Schutz AK, Vagt T, Huber M, Ovchinnikova OY, Cadalbert R, Wall J, Guntert P, Bockmann A, Glockshuber R, Meier BH (2015) Atomic-resolution three-dimensional structure of amyloid beta fibrils bearing the Osaka mutation. Angew Chem Int Ed 54:331–335.

25. Colvin MT, Silvers R, Frohm B, Su Y, Linse S, Griffin RG (2015) High resolution structural characterization of Abeta42 amyloid fibrils by magic angle spinning NMR. J Am Chem Soc 137:7509–7518.

26. Fitzpatrick AWP, Falcon B, He S, Murzin AG, Murshudov G, Garringer HJ, Crowther RA, Ghetti B, Goedert M, Scheres SHW (2017) Cryo-EM structures of tau filaments from Alzheimer's disease. Nature 547:185–190.

27. Economou NJ, Giammona MJ, Do TD, Zheng X, Teplow DB, Buratto SK, Bowers MT (2016) Amyloid beta-protein assembly and Alzheimer's disease: Dodecamers of Abeta42, but not of Abeta40, seed fibril formation. J Am Chem Soc 138:1772–1775.

28. Laganowsky A, Liu C, Sawaya MR, Whitelegge JP, Park J, Zhao ML, Pensalfini A, Soriaga AB, Landau M, Teng PK, Cascio D, Glabe C, Eisenberg D (2012) Atomic view of a toxic amyloid small oligomer. Science 335:1228–1231.

29. Riek R, Eisenberg DS (2016) The activities of amyloids from a structural perspective. Nature 539:227–235.

30. Tycko R (2006) Molecular structure of amyloid fibrils: insights from solid-state NMR. Quart Rev Biophys 39:1–55.

31. Do TD, Economou NJ, Chamas A, Buratto SK, Shea JE, Bowers MT (2014) Interactions between amyloid-beta and Tau fragments promote aberrant aggregates: implications for amyloid toxicity. J Phys Chem B 118:11220–11230.

32. Ganguly P, Do TD, Larini L, LaPointe NE, Sercel AJ, Shade MF, Feinstein SC, Bowers MT, Shea JE (2015) Tau assembly: the dominant role of PHF6 (VQIVYK) in microtubule binding region repeat R3. J Phys Chem B 119:4582–4593.

33. Pawar AP, Dubay KF, Zurdo J, Chiti F, Vendruscolo M, Dobson CM (2005) Prediction of "aggregation-prone" and "aggregation-susceptible" regions in proteins associated with neurodegenerative diseases. J Mol Biol 350:379–392.

34. Tartaglia GG, Pawar AP, Campioni S, Dobson CM, Chiti F, Vendruscolo M (2008) Prediction of aggregation-prone regions in structured proteins. J Mol Biol 380:425–436.

35. Tjernberg L, Hosia W, Bark N, Thyberg J, Johansson J (2002) Charge attraction and beta propensity are necessary for amyloid fibril formation from tetrapeptides. J Biol Chem 277:43243–43246.

36. Kim W, Hecht MH (2006) Generic hydrophobic residues are sufficient to promote aggregation of the Alzheimer's Abeta42 peptide. Proc Natl Acad Sci USA 103:15824–15829.

37. Gazit E (2002) A possible role for pi-stacking in the self-assembly of amyloid fibrils. FASEB J 16:77–83.

38. Truex NL, Wang Y, Nowick JS (2016) Assembly of peptides derived from beta-sheet regions of beta-amyloid. J Am Chem Soc 138:13882–13890.

39. Xiao Y, Ma B, McElheny D, Parthasarathy S, Long F, Hoshi M, Nussinov R, Ishii Y (2015) 1–42) fibril structure illuminates self-recognition and replication of amyloid in Alzheimer's disease. Nat Struct Mol Biol 22:499–505. Abeta(

40. Goldschmidt L, Teng PK, Riek R, Eisenberg D (2010) Identifying the amylome, proteins capable of forming amyloid-like fibrils. Proc Natl Acad Sci USA 107:3487–3492.

41. Thompson MJ, Sievers SA, Karanicolas J, Ivanova MI, Baker D, Eisenberg D (2006) The 3D profile method for identifying fibril-forming segments of proteins. Proc Natl Acad Sci USA 103:4074–4078.

42. Do TD, LaPointe NE, Nelson R, Krotee P, Hayden EY, Ulrich B, Quan S, Feinstein SC, Teplow DB, Eisenberg D, Shea J-E, Bowers MT (2016) Amyloid β-protein C-terminal fragments: Formation of cylindrins and β-barrels. J Am Chem Soc 138:549–557.

43. Do TD, Economou NJ, LaPointe NE, Kincannon WM, Bleiholder C, Feinstein SC, Teplow DB, Buratto SK, Bowers MT (2013) Factors that drive peptide assembly and fibril formation: Experimental and theoretical analysis of Sup35 NNQQNY mutants. J Phys Chem B 117:8436–8446.

44. Do TD, LaPointe NE, Sangwan S, Teplow DB, Feinstein SC, Sawaya MR, Eisenberg DS, Bowers MT (2014) Factors that drive peptide assembly from native to amyloid structures: experimental and theoretical analysis of [Leu-5]-enkephalin mutants. J Phys Chem B 118:7247–7256.

45. Kuhlman B, Baker D (2000) Native protein sequences are close to optimal for their structures. Proc Natl Acad Sci USA 97:10383–13460.

46. Petkova AT, Yau WM, Tycko R (2006) Experimental constraints on quaternary structure in Alzheimer's beta-amyloid fibrils. Biochemistry 45:498–512.

47. Miller DL, Papayannopoulos IA, Styles J, Bobin SA, Lin YY, Biemann K, Iqbal K (1993) Peptide compositions of the cerebrovascular and senile plaque core amyloid deposits of Alzheimer's disease. Arch Biochem Biophys 301:41–52.

48. Iwatsubo T, Mann DM, Odaka A, Suzuki N, Ihara Y (1995) Amyloid beta protein (A beta) deposition: a beta 42(43) precedes A beta 40 in Down syndrome. Ann Neurol 37:294–299.

49. Ahmed M, Davis J, Aucoin D, Sato T, Ahuja S, Aimoto S, Elliott JI, Nostrand WEV, Smith SO (2010) Structural conversion of neurotoxic amyloid-β1–42 oligomers to fibrils. Nat Struct Mol Biol 17:561–567.

50. Paravastu AK, Leapman RD, Yau WM, Tycko R (2008) Molecular structural basis for polymorphism in Alzheimer's beta-amyloid fibrils. Proc Natl Acad Sci USA 105:18349–18354.

51. Bleiholder C, Dupuis NF, Wyttenbach T, Bowers MT (2011) Ion mobility-mass spectrometry reveals a conformational conversion from random assembly to β-sheet in amyloid fibril formation. Nat Chem 3:172–177.

52. Seo J, Hoffmann W, Warnke S, Huang X, Gewinner S, Schollkopf W, Bowers MT, von Helden G, Pagel K (2017) An infrared spectroscopy approach to follow beta-sheet formation in peptide amyloid assemblies. Nat Chem 9:39–44.

53. Wyttenbach T, Kemper PR, Bowers MT (2001) Design of a new electrospray ion mobility mass spectrometer. Int J Mass Spectrom 212:13–23.

54. Kemper PR, Dupuis NF, Bowers MT (2009) A new, higher resolution, ion mobility mass spectrometer. Int J Mass Spectrom 287:46–57.